MOLECULAR CRYSTALS
AND
LIQUID CRYSTALS

Molecular Crystals and Liquid Crystals

ISSN: 1542-1406 (Print) 1563-5287 (Online) Journal homepage: http://www.tandfonline.com/loi/gmcl20

Two-step crosslinked liquid-crystalline elastomer with reversible two-way shape memory characteristics

Yuchang Wang, Xuezhen Huang , Jianqi Zhang, Meng Bi, Jindi Zhang, Hongyan Niu, Chensha Li, Haifeng Yu , Binsong Wang & Hongrui Jiang

To cite this article: Yuchang Wang, Xuezhen Huang , Jianqi Zhang, Meng Bi, Jindi Zhang, Hongyan Niu, Chensha Li, Haifeng Yu , Binsong Wang & Hongrui Jiang (2017) Two-step crosslinked liquid-crystalline elastomer with reversible two-way shape memory characteristics, Molecular Crystals and Liquid Crystals, 650:1, 13-22, DOI: 10.1080/15421406.2017.1318025

To link to this article: http://dx.doi.org/10.1080/15421406.2017.1318025

MOLECULAR CRYSTALS AND LIQUID CRYSTALS
2017, VOL. 650, 13–22
https://doi.org/10.1080/15421406.2017.1318025

Taylor & Francis
Taylor & Francis Group

Two-step crosslinked liquid-crystalline elastomer with reversible two-way shape memory characteristics

Yuchang Wang[a], Xuezhen Huang[b], Jianqi Zhang[c], Meng Bi[a], Jindi Zhang[a], Hongyan Niu[a], Chensha Li[d], Haifeng Yu[e], Binsong Wang[a], and Hongrui Jiang[b]

[a]Key Laboratory of Chemical Engineering Process and Technology for High-Efficiency Conversion, School of Chemistry and Material Sciences, Heilongjiang University, Harbin, P. R. China; [b]Department of Electrical and Computer Engineering, University of Wisconsin-Madison, Wisconsin, USA; [c]Key Laboratory of Nanosystem and Hierarchical Fabrication, National Center for Nanoscience and Technology, Beijing, P. R. China; [d]Key Laboratory of Functional Inorganic Material Chemistry, Ministry of Education of the People's Republic of China, Heilongjiang University, Harbin, P. R. China; [e]Key Laboratory of Polymer Chemistry and Physics of Ministry of Education, Peking University, Beijing, P. R. China

ABSTRACT
Liquid-crystalline elastomers (LCEs) possess large and equilibrium reversible anisotropic dimensional change in response to applied stimuli. The deformation behavior demonstrated by current LCE materials under the stimuli are generally determined by their own geometries and the alignment distributions of liquid crystal (LC) units in the LCE matrices. Here we report a LCE whose synthesis was through a two-stage crosslinking coupled with a mechanical reshaping process, where the shape was mechanically reset before the final crosslinking. It demonstrated reversible memory and change between the initial geometries formed during the first crosslinking stage and any reshaped geometries under the stimuli. Its deformation is not influenced by the geometries and the alignment distributions of LC units in the LCE matrix. This characteristic in LCEs holds promise in a wide range of application researches requiring sophisticated functions and smart structures.

KEYWORDS
Liquid crystalline elastomer; Nematic structure; Shape memory effect; Smart deformable material; Sophisticated deformation

Introduction

Smart polymer deformable materials have attracted wide attention due to their capability of shape change upon external stimuli such as heat, light, electric field or magnetic field, high mechanical flexibility, light weight, low cost, and low-noise operation, which leads to applications in deployable structures, microdevices, biomedical devices and actuators [1]. Liquid-crystalline elastomers (LCEs), which are liquid crystalline polymer networks (LCNs) with lightly cross-linked networks, are a type of smart polymer deformable material with the

---

CONTACT Chensha Li 2015068@hlju.edu.cn Key Laboratory of Functional Inorganic Material Chemistry, Ministry of Education of the People's Republic of China, Heilongjiang University, Harbin 150080, P. R. China; Haifen Yu, yuhaifeng@pku.edu.cn, Key Laboratory of Polymer Chemistry and Physics of Ministry of Education, Peking University, Beijing 100871, P. R. China; Binsong Wang, 2005037@hlju.edu.cn, Key Laboratory of Chemical Engineering Process and Technology for High-Efficiency Conversion, School of Chemistry and Material Sciences, Heilongjiang University, Harbin 150080, P. R. China; Hongrui Jiang, hongrui@engr.wisc.edu, Department of Electrical and Computer Engineering, University of Wisconsin-Madison, WI 53706, USA.

Color versions of one or more of the figures in the article can be found online at www.tandfonline.com/gmcl.

Yuchang Wang, Xuezhen Huang, and Jianqi Zhang contributed equally to this work.

Supplemental data for this article can be accessed on the publisher's website.

appealing combination of physical properties that makes them stand out from other materials. LCEs possess both the self-organization nature of liquid crystal (LC) systems and the flexibility of rubber elasticity, the conjunction of which enables large and equilibrium reversible anisotropic dimensional change of LCEs in response to applied stimuli. Many novel and interesting physical effects arise from the coupling of the mobile anisotropic properties of LC units to the rubber elastic matrices [2–4].

As the liquid-crystalline assembly undergoes a nematic-isotropic transition, it loses the associated anisotropy of the polymer backbone chains induced by the coupling to the nematic order, resulting in a macroscopic deformation of the LCE or LCN material [2–5]. Moreover, the nematic phase state of a LCE or LCN matrix is formed by direction-dependent alignment of the LC units in the matrix network, which paves the way for correlating controllable anisotropic shape change to the alignment pattern. Due to the uniaxial alignment of LC units, LCE or LCN materials with uniaxial nematic structure generally exhibit reversible uni-directional main deformations, such as contraction/elongation [6–9] or bending/unbending [9–14], under applied stimuli. Researchers have synthesized LCNs with the alignment of LC units splayed or twisted and distributed through the thickness [15–21], or more complex topology distribution in LCN matrices [22–24] by using the patterned alignment layers to drive the orientations of LC units; the LCNs then exhibited reversible deformation of large amplitude bending, coiling, twisting, helix, sophisticated curving or surface topography under applied stimuli. Through a microfluidic process [25–27], complex alignment distributions could be formed in synthesized LCE microsized particles by the effect of microfluidic mechanics, resulting in complex reversible shape change (aspect ratios) of these particles. Induced by multi-directional magnetic field or inhomogeneous stress field [28, 29], complex alignment distributions of LC units were also formed before or during the crosslinking processes, and thus the fabricated LCE materials demonstrated complex reversible shape change under applied stimuli. However, these resultant changes in shape during the nematic-isotropic transition are determined by their original geometries and the alignment distributions of LC units, etc.

Some recent publications have reported on shape memory in LCNs by exploiting glassy deformations [30–32]. Here, we report a LCE whose synthesis was through a two-stage crosslinking coupled with a mechanical reshaping process, the shape was mechanically reset after the first crosslinking, followed by the second crosslinking to fix the reset shape and alignment distribution of LC units. This LCE material demonstrated a characteristic of reversible two-way shape memory: it was able to change reversibly between the initial geometries formed during the first crosslinking and any reshaped geometries with different alignment distribution of LC units during the nematic-isotropic transition. This characteristic in LCEs may bring forth the potential to develop sophisticated smart devices and structures that can switch between different designed forms and shapes for different functions.

Experimental section

The side-chain nematic LCE network with polysiloxane backbone was synthesized by referencing the previous reported work [2]. The Si–H bonds in the polysiloxane backbone reacted, using the platinic acid catalyst, with the terminal vinyl groups of the mesogenic rod-like molecules and the two-functional crosslinkers by hydrosilation. As shown in Scheme 1, after the noncomplete hydrosilylation reaction, the sample was mechanically reshaped, which also simultaneously contributed the alignment distribution of mesogens in LCE matrix. The second crosslinking process made the completion of the hydrosilylation reaction, fixed the reset

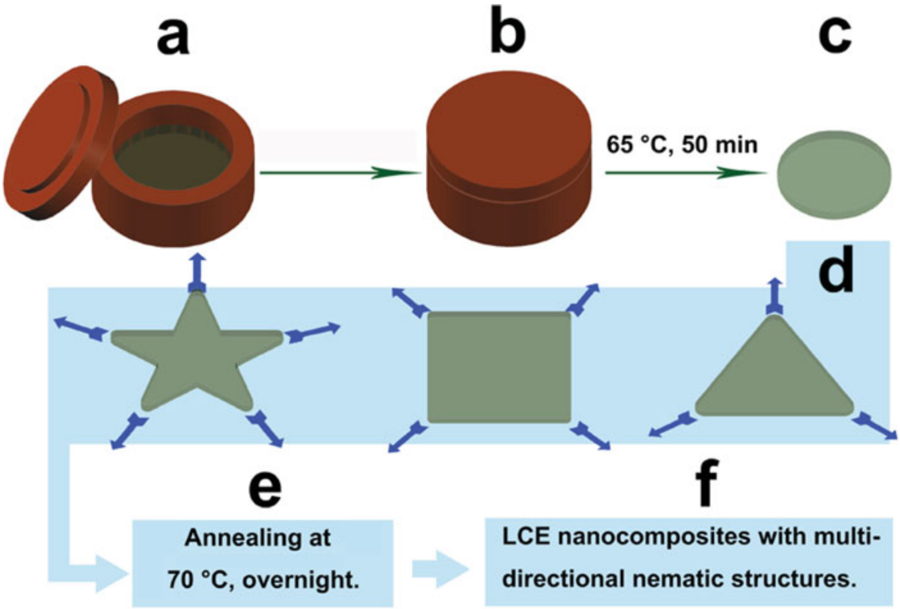

Scheme 1. Synthetic route for the LCE/GO nanocomposites with multi-orientation nematic structures. (a) Casting reactive solution mixture into the mold. (b) The first crosslinking stage. (c) The obtained partially crosslinked gel (containing GO) with the initial geometry—a disc shape with the diameter of 2.0 cm. (d) The shape-resetting process. (e) The second crosslinking stage. (f) Obtaining the multi-orientation nematic LCE/GO nanocomposites with the permanent reshaped geometries of regular triangle, square, and five-pointed star, respectively.

shape and nematic phase structure. Here the reaction system was ahead filled with graphene-oxide (GO), so that the prepared LCE material contained GO which acted as a photo-thermal transforming agent for the photo-thermal-mechanical actuation of LCE material [33].

The pendant mesogenic group: 4-methoxyphenyl 4-(but-3-en-1-yloxy)benzoate and di-functional crosslinking group: 1, 4-bis(undec-10-en-1-yloxy)benzene were synthesized as reported in our prior work [34]. The polymer backbone: PMHS with approximately 60 Si–H units per chain was from ACROS Chemicals, Belgium. The catalyst solution was prepared by dissolving 0.025 g of the dichloro (1, 5-cyclooctadiene) platinum (II) (Sigma-Aldrich) in 2 ml of dichloromethane, then mixed with 20 ml of toluene. 0.25 mg of GO was dispersed into the reaction mixture solution, prepared by dissolving 0.048 g of PMHS, 0.2 g of 4-methoxyphenyl 4-(but-3-en-1-yloxy)benzoate (0.672 mmol) and 0.027 g of 1, 4-bis(undec-10-en-1-yloxy)benzene (0.066 mmol) into 0.8 mL of toluene, and then ultrasonicated for 2 min. 50 μL of catalyst solution was then added into the reaction mixture solution. Next, the solution was cast into a round polytetrafluoroethylene (PTFE) mold with the diameter and depth of 3.0 cm and 0.5 cm, respectively (Scheme 1(a)). The mold was subsequently covered by a cap and heated in an oven at 65°C for 50 min for partial crosslinking (first crosslinking stage) (Scheme 1(b)). After the mold was cooled down to room temperature, 3 mL of hexane was poured into the mold to facilitate the removal of the partially crosslinked swollen gel. The partially crosslinked GO-contained disc-shaped swollen gel was carefully removed from the mold and dried in air for 40 min. As the toluene contained in the gel gradually evaporated, the disc-shaped gel kept shrinking and eventually achieved a disc-shape with a stable diameter of 2.0 cm (Scheme 1(c)), which was the initial geometry. To the reshaping process (Scheme 1(d)): The disc-shaped gel was drawn from three, four or five points, evenly-spaced on its circumference along the three, four or five radial directions with mutual angles of 120°, 90°, or 72° under a constant tensile force provided by 3.5 g of loads in each direction. After 12 hours of drawing, the disc-shaped gel became a regular triangle with a stable dimension of 3 cm in side length, or a square with a stable dimension of 3 cm in side length, or a five-pointed star with a stable dimension of 2.7 cm in distance between every two alternate vertices, and 0.6 mm in thickness. The nanocomposite gel with the reset shape was annealed at 70°C overnight to complete the crosslinking reaction (second crosslinking stage) (Scheme 1 (e)). Through above procedure, the nematic LCE/GO nanocomposites (with an effective cross-linking density of 16.5% and GO content of 0.1 wt%) with the permanent reshaped geometries of regular triangle, square and five-pointed star were prepared, respectively (Scheme 1(f)). We also prepared the nematic LCE/GO nanocomposites with the permanent reshaped geometries of six-pointed-star and eight-pointed-star, respectively, following the same procedure.

Results and discussion

Using polarizing optical microscopy (POM, Nikon Instruments, SMZ 1500, Melville, NY), the distribution of alignments of the mesogens in the LCE matrix was evaluated by measuring the transmittance of a probe light through two crossed polarizers and a LCE/GO nanocomposite between them. The POM observation of a square-shaped nematic LCE/GO nanocomposite, as shown in Figure 1(a)–(c), evidenced the alignment distribution of mesogens in its LCE matrix, as shown in Figure 1(d). The alignments in each of the four angles were approximately along and symmetrically distributed with respect to one diagonal. The alignments in the areas close to the diagonals were essentially parallel to them, and gradually inclined towards the sides away from the diagonals. In the middle area between every two adjacent angles, the alignment was basically parallel to the shared side of the two angles. There existed the polydomain areas located at the center and contiguous to the four sides. When the sample was rotated, the poly-domain areas were always opaque due to scattering of light, while periodic change between dark (due to light extinction) and bright images could be observed in alignment areas. When

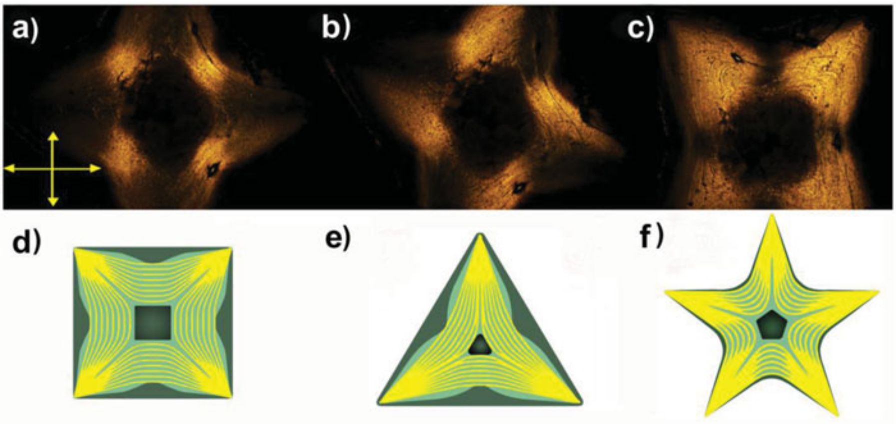

Figure 1. (a)–(c) POM images showing alignment distribution of mesogens in LCE matrix of a square LCE/GO nanocomposite: (a) The two diagonals are aligned with the two polarization directions, respectively. Inserted crossarrows illustrate the polarization directions of the two polarizers. (b) Clockwise rotation of the sample by 15° from (a). (c) Clockwise rotation of the sample by 45° from (a). The two diagonals are at 45° with respect to the two polarization directions, respectively. (d)–(f) The schematic alignment distributions of the LCE/GO nanocomposites with the shape of square, (d), regular triangle, (e), and five-pointed star, (f), respectively. Their alignment distributions are illustrated by yellow lines; the dark green areas are polydomain areas.

the two diagonals of the square sample were respectively parallel to the two polarization directions shown in Figure 1(a), the alignments in the four angles were approximately along the polarization directions, resulting in a low transmittance of light (dark) in these areas. The lowest transmittance appeared around the diagonals. Light transmittance increased towards the sides, because the alignments there gradually inclined away from the polarization directions. The middle part between every two adjacent angles had the highest transmittance (brightest) as alignments in these areas were 45° with respect to the two polarization directions. Since the alignments were symmetrically distributed with respect to the diagonals in every angle, when the sample was rotated from the initial state in Figure 1(a), bright areas and dark areas would start to alternate. Figure 1(b) shows such alternation, when the sample was rotated clockwise by 15°. Areas with alignments now parallel to the polarization directions displayed lowest transmittance (dark), while other areas with alignments deviated from the polarization directions had higher transmittance (bright). Figure 1(c) shows when the sample was further rotated till the two diagonals intersected with the two polarization directions at 45°. The four angles became bright, while the middle areas between every two neighboring angles became dark. The POM measurement was consistent with the nematic structure in the LCE matrix as depicted in Figure 1(d). Two other multi-orientation nematic LCE/GO nanocomposites prepared in different shapes (regular triangle and star) showed similar POM characteristics (see Supplementary Figure. S1 and Figure. S2), and their obtained alignment distributions are shown in Figure 1(e) and (f).

X-ray diffraction (XRD) was used to measure the alignment distribution of LCE. The measurement was mainly performed using a rotating anode X-ray system, Cu Kα beam filtered by a confocal mirror ($\lambda = 1.54$ Å, X-ray power = 2.7 kW) and a two-dimensional image plate system (2540 × 2540 pixels, 50 μm resolution). As shown in Figure 2, the azimuthal intensity maxima at wide-angle reflections indicate alignments of mesogens in LCE matrix. In position ①, ②, and ③, the locations of the wide-angle reflection are orthogonal to the alignments of the mesogens, while only halos are observed in position ④ and ⑤. The XRD measurements confirmed the nematic structure in LCE matrix as depicted in Figure 1(d).

The reversible two-way shape memory characteristic was observed in this LCE, as shown in Figure 3 and Supplementary Video 1–3. Here the GO dispersed inside the LCE matrix absorbed and converted photon energy into thermal energy to heat the LCE matrix, converting the nematic structure to isotropic state, hence the deformation. Under the IR light

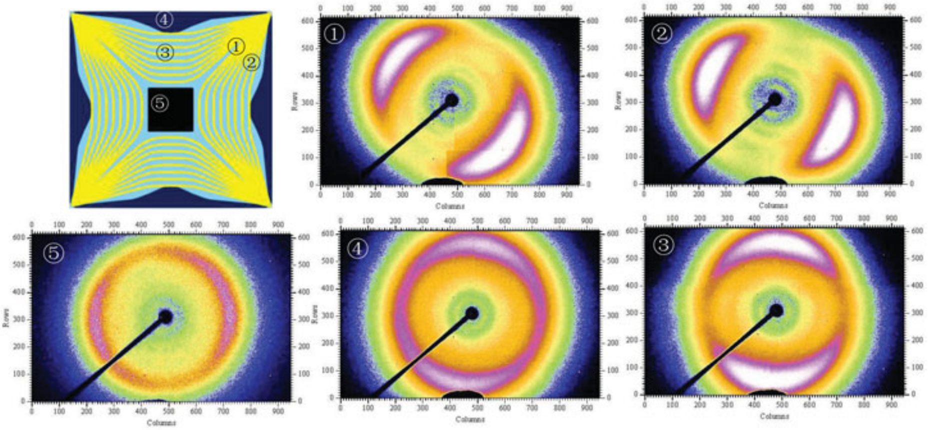

Figure 2. XRD patterns at different positions of the square LCE/GO nanocomposite.

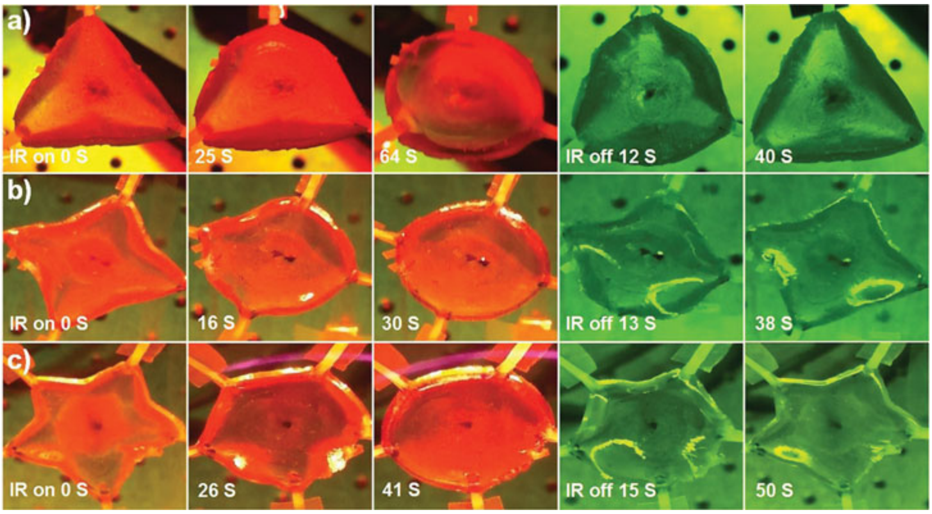

Figure 3. Photos showing the reversible photo-driven shape memory of the nematic LCE/GO nanocomposites with geometries of (a) regular triangle, (b) square, and (c) five-pointed star. All these LCE/GO nanocomposites change to their initial geometry which is a disc shape with the diameter of 2.0 cm in several tens of seconds under an IR irradiation of 2.4 W/cm^2, and recover to their reshaped geometries, respectively in several tens of seconds after the IR irradiations are removed.

(Hotspot, Model H. S. 250.3, I^2R, Cheltenham, PA) with an intensity of 2.4 W/cm^2, the LCE/GO nanocomposites with the geometries of regular triangle, square and five-pointed star all changed to their initial shape which was a disc shape with the diameter of 2.0 cm within several tens of seconds. After the IR irradiation was removed, the nematic structure and alignment distributions of mesogens were restored in the LCE matrix as the temperature decreased. The LCE/GO nanocomposites thus resumed their respective geometries and dimensions. Six-pointed- and eight-pointed-star shaped LCE/GO nanocomposites also demonstrated the same reversible two-way shape memory characteristic (see Supplementary Figure. S3-S4).

One main cause that brings about this reversible two-way shape memory characteristic of this LCE should be attributed to its synthesis process. The mechanic-induced molecular alignment effect and the phase-variation-induced deformation of this LCE are schematically illustrated in Scheme 2. The partially crosslinked gel synthesized during the first crosslinking stage contained plenty of micrometer-sized small domains which although individually disciplined the molecular directors of the inside mesogens in a unidirectional way, could

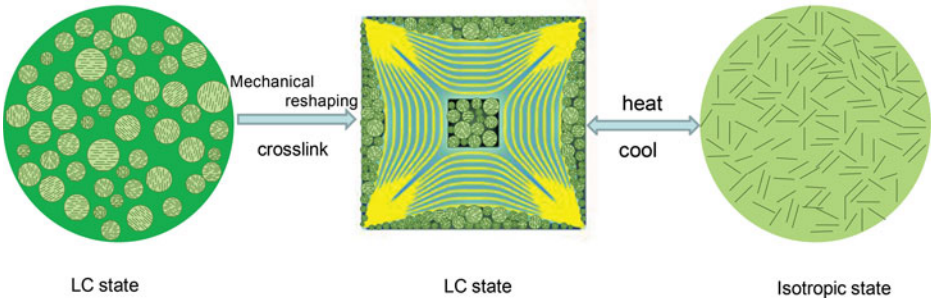

Scheme 2. Illustration of the mechanic-induced molecular alignment effect and the phase-variation-induced deformation mechanism of the LCE.

not unify the molecular arrangements of all the domains in an ordered manner, so that the mesogens on average were randomly oriented. During the mechanical reshaping process, the stress field on the precross-linked gel could force the mesogens to change the multidomain molecular packing into monodomain alignments (the polydomain structure in the blind areas of stress field could not be changed). The alignment distribution formed by the mechanical reshaping process was eventually fixed by second crosslinking stage, and the reset shape of LCE matrix was also fixed by the completely crosslinked network. When the stimulus was applied to trigger the LC-to-isotropic phase transition, all the mesogens behaved in a random arrangement manner, which was similar to the polydomain molecular packing from a macroscopic view. Thus, the whole LCE tended to recover its initial shape of precross-linked gel. The second main cause should be that the partially crosslinked gel synthesized in the first crosslinking stage was fully elastic and no plastic strain occurred during the mechanical reshaping process, this ensured that the material could fully return back to its initial shape after the LC-to-isotropic phase transition. With these two reasons, different reshaped LCE materials can all change back to the same initial shape after the nematic-isotropic transition. After the isotropic-nematic transition, the recovering of topology of the LC network, induced by the internal stress originating from cross links between polymer backbones [35, 36], drove the LCE material to its reset shape.

This reversible two-way shape memory effect exists not only in this LCE with uni-axial nematic structure (which was also demonstrated in our experiments), but also in it with any multi-orientation nematic structure, as demonstrated in this work, and is not limited by the material shape and the way of mechanical reshaping process.

When the deformation of the LCE was partly restricted, it demonstrated other sophisticated deformations under the stimuli which were stemmed from the multi-orientation nematic structure in LCE matrix. As shown in Figure 4, one LCE/GO nanocomposite shaped as a six-pointed star was adhered to a gummed tape cut into the same shape on the bottom side. When irradiated from the top using the IR light source, the deformation of the bottom side was restricted by the gummed tape, while other areas not constrained could deform normally. As a result, all the points bent up until their vertices approached right above the center of the six-pointed star in tens of seconds under the IR irradiation of 2.4 W/cm^2, and then unfolded back to their initial states, also in tens of seconds, after the IR irradiation was removed, mimicking a water lily opening and closing up its petals.

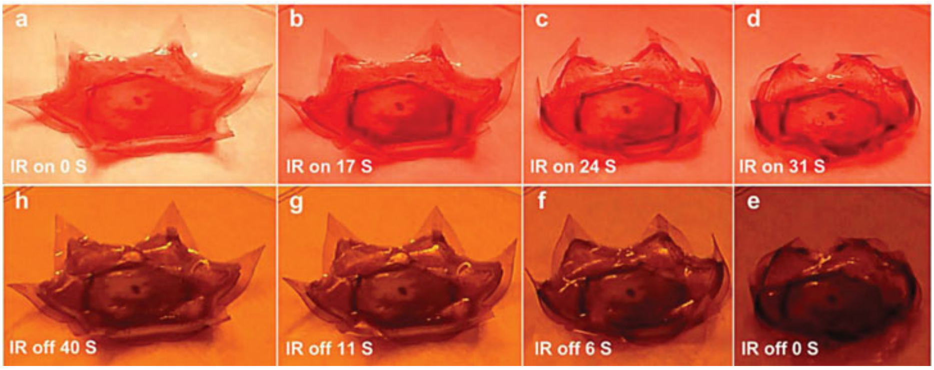

Figure 4. Photos of the reversible 3D multi-directional deformation of a six-pointed-star LCE/GO nanocomposite. With its bottom surface constrained by a piece of gummed tape, the points of the LCE/GO nanocomposite completely curl up after about 30 seconds under an IR irradiation of 2.4 W/cm^2, and unfold back to their initial states within 40 seconds after the IR irradiation is removed.

Conclusions

We report a LCE synthesized by a method of two-stage crosslinking, coupled with a mechanical reshaping process. The alignment distribution of LC units was defined by the shape resetting process and varied with different reset shapes. The material could maintain fully reversible memory between the initial shape and any reset one, and possessed spontaneous reversible change between them under applied stimuli. The mechanism is thought to be a combination of the memory effects of elastomer and LC network, the memory effect of elastomer made the material to return back to the initial shape when the ordered network disappeared, the memory effect of LC network led to the recovering of topology of the LC network after the isotropic-nematic transition, and thus drove the material to its reset shape. This reversible memory is not limited by material shape, shape resetting process and the alignment distribution of LC units in LCE matrix. The LCE material with this characteristic not only holds promise in application researches in the current focused areas for LCE and LCN materials, such as artificial muscles [37–40], robots [41, 42] and actuators [18, 43–47], but also in much wider application researches that demand sophisticated and multifunctional structures, such as developing smart devices which can switch between different designed forms and shapes for different functions.

Acknowledgments

This research utilized NSF-supported shared facilities at the University of Wisconsin. The authors thank G. Lin for help in video preparation, N. L. Abbott, Z. Q. Yang and C. Lo for academic communications.

Funding

This work was funded by the University of Wisconsin – Madison Vilas Associates Program supported by the Vilas Trustees, and partly by Wisconsin Institutes for Discovery and the U.S. National Science Foundation under Grant ECCS 0702095.

Conflict of interest

The authors declare no competing financial interest.

Table of content entry

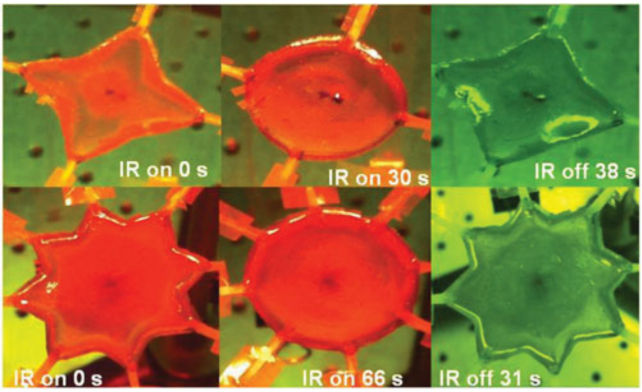

The title systems show the reversible two-way memory and change between the initial and the reshaped geometries under photo-triggering of the LCE materials with different alignment distribution of mesogens. This characteristic not only holds promise in application researches in the current focused areas for LCE materials, such as artificial muscles, robots and actuators, but also in much wider application researches requiring multi-functional structures.

ORCID

Xuezhen Huang http://orcid.org/0000-0003-0020-4735
Haifeng Yu http://orcid.org/0000-0003-0398-5055
Hongrui Jiang http://orcid.org/0000-0001-8468-5454

References

[1] Ikeda, T., Mamiya, J.-I., & Yu, Y. (2007). *Angew. Chem. Int. Edit.*, *46*, 506–528.
[2] Warner, M., & Terentjev, E. M. (2007). *Liquid Crystal Elastomers*, Oxford University Press: Oxford, UK.
[3] Ohm, C., Brehmer, M., & Zentel, R. (2010). *Adv. Mater.*, *22*, 3366–3387.
[4] Yu, H., & Ikeda, T. (2011). *Adv. Mater.*, *23*, 2149–2180.
[5] Yu, H. (2014). *J. Mater. Chem. C.*, *2*, 3047–3054.
[6] Zander, F., & Finkelmann, H. (2010). *Macromol. Chem. Phys.*, *211*, 1167–1176.
[7] Ohm, C., Morys, M., Forst, F. R., Braun, L., Eremin, A., Serra, C., et al. (2011). *Soft Matter.*, *7*, 3730–3734.
[8] Liu, W., Guo, L.-X., Lin, B.-P., Zhang, X.-Q., Sun, Y., et al. (2016). *Macromolecules*, *49*, 4023–4030.
[9] Wang, M., Sayed, S. M., Guo, L.-X., Lin, B.-P., Zhang, X.-Q., et al. (2016). *Macromolecules*, *49*, 663–671.
[10] Kondo, M., Yu, Y., & Ikeda, T. (2006). *Angew. Chem.-Int. Edit.*, *45*, 1378–1382.
[11] Yu, Y., Maeda, T., Mamiya, J.-I., & Ikeda, T. (2007). *Angew. Chem.-Int. Edit.*, *46*, 881–883.
[12] Li, C., Lo, C.-W., Li, C., Zhu, D., Liu, Y., et al. (2009). *Macromol. Rapid Commun.*, *30*, 1928–1935.
[13] Yoshino, T., Kondo, M., Mamiya, J., Kinoshita, M., Yu, Y., et al. (2010). *Adv. Mater.*, *22*, 1361–1363.
[14] Wang, W., Sun, X., Wu, W., Peng, H., & Yu, Y. (2012). *Angew. Chem. Int. Edit.*, *51*, 4644–4647.
[15] Harris, K. D., Cuypers, R., Scheibe, P., Oosten, C. L. V., et al. (2005). *J. Mater. Chem.*, *15*, 5043–5048.
[16] Mol, G. N., Harris, K. D., Bastiaansen, C. W. M., & Broer, D. J. (2005). *Adv. Funct. Mater.*, *15*, 1155–1159.
[17] Harris, K. D., Bastlaansen, C. W. M., Lub, J., & Broer, D. J. (2005). *Nano Lett.*, *5*, 1857–1860.
[18] Oosten, C. L. V., Bastiaansen, C. W. M., & Broer, D. J. (2009). *Nat. Mater.*, *8*, 677–682.
[19] Wie, J. J., Lee, K., Smith, M. L., Vaia, R. A., & White, T. J. (2013). *Soft Matter.*, *9*, 9303–9310.
[20] Sawa, Y., Ye, F., Urayama, K., Takigawa, T., Vianney, G.-P., et al. (2011). *Proc. Natl Acad. Sci. USA.*, *108*, 6364–6368.
[21] Iamsaard, S., Abhoff, S. J., Matt, B., Kudernac, T., Cornelissen, J. L. M., et al. (2014). *Nat. Chem.*, *6*, 229–235.
[22] Haan, L. T. D., Sánchez-Somolinos, C., Bastiaansen, C. M. W., Schenning, A. P. H. J., et al. (2012). *Angew. Chem. Int. Ed.*, *51*, 12469–12472.
[23] Mcconney, M. E., Martinez, A., Tondiglia, V. P., Lee, K. M., Langley, D., et al. (2013). *Adv. Mater.*, *25*, 5880–5885.
[24] Haan, L. T. D., Gimenez-Pinto, V., Konya, A., Nguyen, T. S., Verjans, J. M. N., et al. (2014). *Adv. Funct. Mater.*, *24*, 1251–1258.
[25] Ohm, C., Serra, C., & Zentel, R. (2009). *Adv. Mater.*, *21*, 4859–4862.
[26] Ohm, C., Kapernaum, N., Nonnenmacher, D., Giesselmann, F., Serra, C., et al. (2011). *J. Am. Chem. Soc.*, *133*, 5305–5311.
[27] Fleischmann, E.-K., Liang, H.-L., Kapernaum, N., Giesselmann, F., Lagerwall, J., et al. (2012). *Nat. Commun.*, *3*, 1178–1185.
[28] Schuhladen, S., Preller, F., Rix, R., Petsch, S., Zentel, R., et al. (2014). *Adv. Mater.*, *26*, 7247–7251.
[29] Ahn, C., Liang, X., & Cai, S. (2015). *Extreme Mech. Lett.*, *5*, 30–36.
[30] Lee, K. M., Koerner, H., Vaia, R. A., Bunning, T. J., & White, T. J. (2011). *Soft Matter.*, *7*, 4318–4324.
[31] Lee, K. M., Bunning, T. J., & White, T. J. (2012). *Adv. Mater.*, *24*, 2839–2843.
[32] Kumar, K., Schenning, A. P. H. J., Broer, D. J., & Liu, D. Q. (2016). *Soft Matter.*, *12*, 3196–3201.

[33] Jiang, H., Li, C., & Huang, X. (2013). *Nanoscale*, *5*, 5225–5240.
[34] Li, C., Liu, Y., Lo, C.-W., & Jiang, H. (2011). *Soft Matter.*, *16*, 7511–7516.
[35] Hiraoka, K., Sagano, W., Nose, T., & Finkelmann, H. (2005). *Macromolecules*, *38*, 7352–7357.
[36] Menzel, A. M. (2015). *Phys. Rep.*, *554*, 1–45.
[37] Wermter, H., & Finkelmann, H. (2001). *E-Polymers*, *1*, 111–123.
[38] Li, M. H., & Keller, P. (2006). *Phil. Trans. R. Soc. A.*, *364*, 2763–2777.
[39] Yamada, M., Kondo, M., Miyasato, R., Naka, Y., Mamiya, J., et al. (2009). *J. Mater. Chem.*, *19*, 60–62.
[40] Marshall, J. E., Gallagher, S., Terentjev, E. M., & Smoukov, S. K. (2014). *J. Am. Chem. Soc.*, *136*, 474–479.
[41] Cheng, F., Yin, R., Zhang, Y., Yen, C.-C., & Yu, Y. (2010). *Soft Matter.*, *6*, 3447–3449.
[42] Kohlmeyer, R. R., & Chen, J. (2013). *Angew. Chem.-Int. Edit.*, *52*, 9234–9237.
[43] Camacho-Lopez, M., Finkelmann, H., Muhoray, P. P., & Shelley, M. (2004). *Nature Mater.*, *3*, 307–310.
[44] Yang, H., Buguin, A., Taulemesse, J. M., Kaneko, K., Mery, S. S., et al. (2009). *J. Am. Chem. Soc.*, *131*, 15000–15004.
[45] Sánchez-Ferrer, A., Fischl, T., Stubenrauch, M., Albrecht, A., Wurmus, H., et al. (2011). *Adv. Mater.*, *23*, 4526–4530.
[46] Li, C., Liu, Y., Huang, X., & Jiang, H. (2012). *Adv. Funct. Mater.*, *22*, 5166–5174.
[47] Torras, N., Zinoviev, K. E., Esteve, J., & Sánchez-Ferrer, A. (2013). *J. Mater. Chem. C.*, *1*, 5183–5190.